PERGAMON

International Journal of Heat and Mass Transfer 43 (2000) 2075–2088

International Journal of HEAT and MASS TRANSFER

www.elsevier.com/locate/ijhmt

Combustion modeling of turbulent jet diffusion H_2/air flame with detailed chemistry

X. Zhou*, Z. Sun, G. Brenner, F. Durst

Lehrstuhl für Strömungsmechanik, Universität Erlangen-Nürnberg, D-91058 Erlangen, Germany

Received 19 March 1999; received in revised form 21 September 1999

Abstract

In the present paper, turbulent jet diffusion flames are investigated numerically using a finite volume method for the solution of the Navier–Stokes and reaction equations governing the problem. The method is based on a finite volume discretization and the SIMPLE approach for velocity and pressure coupling. For validation of the modeling of turbulence and numerical method, results are shown for an inert turbulent jet flow. Different versions of the standard k–ε turbulence model including the Rodi correction are compared with experimental results by Panchapakesan and Lumley. The focus is on the investigation of an axisymmetric turbulent hydrogen/air diffusion flame using a time-dependent numerical model with a detailed chemical mechanism. The chemical reactions are described by nine species and 16 or 17 pairs of elementary steps. The transport and thermodynamic physical properties for each species and gas mixture are obtained from the CHEMKIN-II package. An algebraic correlation closure (ACC) model is used for the coupling of turbulence and chemistry. The temperature and major species (H_2, O_2, H_2O, N_2) distributions are in good agreement with the experimental measurements. The numerical results obtained from the detailed chemistry calculations depend on how the turbulent diffusion coefficients are selected for the species and energy equations.

Keywords: Turbulent jet; Diffusion flame; Detailed chemistry

1. Introduction

Non-premixed (or diffusion) flames have been widely applied in industrial process systems, such as large-scale glass-melting furnaces. Both numerical and experimental investigations of turbulent diffusion flames have been the subject of extensive research during recent years, because they are very important for the understanding of the complex interactions between the turbulent flow and chemical reactions.

The turbulent round jet of constant-density is a simple flow that can be used to verify models for other more complex situations such as combusting jets. Large amount of existing work about the isothermal circular jets [1–4] can supply valuable experimental and theoretical data to evaluate the present numerical model. Wygnanski and Fiedler [4], Panchapakesan and Lumley [1] (hereafter referred to as P & L) performed a comprehensive experimental study of the mean velocity, the turbulence stresses and even the third- or fourth-moments of the fluctuations. The k–ε model is still one of the most

* Corresponding author. Department of Engineering, Queen Mary and Westfield College, Mile End Road, London E1 4NS, UK. Tel.: +44-0171-9755555; fax: +44-0181-9833052.
E-mail address: x.zhou@qmw.ac.uk (X. Zhou).

0017-9310/00/$ - see front matter
PII: S0017-9310(99)00293-8

Nomenclature

A_{f_j}	pre-exponential factor in the forward rate constant of the jth reaction
B_{f_j}	temperature exponent in the forward rate constant of the jth reaction
b	half-width of velocity
c_p	mean specific heat at constant pressure
c_{pi}	specific heat at constant pressure of the ith species
C_1, C_2, C_μ	turbulence constants
C_i	molar concentration of the ith species
d, D	nozzle exit diameter
D_{im}	effective molecular diffusion coefficient
E_{f_j}	activation energy in the rate constant of the jth reaction
g	gravitational acceleration speed
G	production term in the turbulent kinetic energy equation
h	mean specific enthalpy of a mixture
h_i	specific enthalpy of the ith species
$h^0_{f_i}$	heat formation of the ith species at reference temperature
k_{f_j}	forward rate constant of the jth reaction
k_{b_j}	backward rate constant of the jth reaction
K_{C_j}	equilibrium constant for the jth chemical reaction
M_i	molecular weight of the ith species
N_r	number of elementary chemical reactions
N_s	number of gaseous species
R	universal gas constant
R_{b_j}	backward rate of progress of the jth reaction
R_{f_j}	forward rate of progress of the jth reaction
S_ϕ	source terms in the general transport equation
t	time
T	temperature
u, v	mean velocity components
U_{in}, U_s	inflow and centreline mean velocity
x, r	cylindrical axial and radial coordinates
Y_i	mass fraction of the ith species

Greek symbols

Γ	general diffusion coefficient in the general transport equation
δ_{ij}	Kronecker delta
k, ε	turbulent kinetic energy and dissipation rate of turbulent kinetic energy
λ	mixture-averaged molecular thermal conductivity
μ	mixture-averaged molecular viscosity
μ_t, μ_{eff}	turbulent and effective eddy viscosity
ν'_{ij}	stoichiometric coefficient of the ith reactant species in the jth reaction
ν''_{ij}	stoichiometric coefficient of the ith product species in the jth reaction
ρ	density
ϕ	general variable
$\dot{\omega}_i$	net rate of creation of the i species by chemical reaction
$\dot{\omega}^+_i$	production rate of the i species by chemical reaction
$\dot{\omega}^-_i$	destruction rate of the i species by chemical reaction
$\sigma_{\tilde{h}}$, $\sigma_{\tilde{Y}}$	turbulent Prandtl number and turbulent Schmidt number
σ_k, σ_ε	turbulence constants

Superscripts

$\bar{}$	Reynolds average
$\sim$	Favre average
$''$	fluctuation

Subscripts

i	ith species
j	jth chemical reaction

popular turbulence models used for the prediction of turbulent flows. The major shortcoming of the standard k–ε model is that it overpredicts the jet spreading rate. Rodi [3] suggested a correction to the standard k–ε model for the free jet shear flows. Reynolds stress turbulence model [5] is a more advanced turbulence model, but it is more complicated to fulfill as compared to the k–ε model and more empirical constants are involved in it which may cause some uncertainty.

The global one-step chemical mechanism still plays an important role in understanding the chemical and physical process of combustion in two- and three-dimensional reacting flows, but it is unable to predict the intermediate species and the pollutant formation. For that reason, the demand of using detailed chemical kinetics is becoming more and more necessary because it can address the major and minor species simultaneously.

Detailed chemistry mechanisms have been successfully applied in modeling jet flames, but most of them are concerned with laminar flows [6–8]. Katta and his

coworkers have simulated and analyzed the vertically laminar H_2/air and CH_4/air jet diffusion flames in great detail using finite-rate chemistry [6,7]. The laminar jet diffusion flames of H_2/N_2–air and $H_2/H_2/N_2$–air have also been investigated by Takagi et al. [8]. The boundary layer type conservation equations were solved. The main problem in turbulent combustion is modeling the source terms of the mean chemical reaction rates. The coupling of turbulence and chemistry can be described by the k–ε turbulence model together with the presumed probability density function (PDF) [9]. The more advanced method is the PDF evolution method [10] where the transport equation can be solved by the Monte-Carlo method. Another kind of turbulence-chemistry coupling is the flamelet model [11] which represents the turbulent flame as an ensemble of laminar steady-state stretched one-dimensional flames. A flamelet library is needed which can result from the popular flames such as the counterflow diffusion flame. A detailed chemistry can be used to generate the relationship of the chemical species concentrations and the mixture fraction as well as the stretch rate. However, whether choosing the scalar dissipation rate or the strain rate as the stretch rate is still questionable for different cases. Kim investigated the turbulent diffusion flames by using detailed chemistry and multiple-time-scale turbulence model [12], but the method has not been widely accepted. The algebraic correlation closure (ACC) [13] model is not very accurate, but it is simple and make the calculation of turbulent combustion with detailed chemistry feasible. Large-eddy-simulation [14–16] or direct numerical simulation [17] can provide a more detailed information about the turbulent reacting flows, but their application in complex flows concerning detailed chemistry is still limited due to limited computer resources.

Some experimental measurements [5,18–20] have been obtained of the turbulent diffusion flames which supply a sound foundation for numerical simulations. A detailed understanding of the interaction of the complex, turbulent, finite-rate chemistry with multi-dimensional fluid dynamics is made possible by the development of numerical combustion models. Detailed comparisons with available experimental data are necessary to verify the mathematical models.

In the present study, the free round jet flow has been first simulated as a test case. Comparisons are carried out between the results of the present simulation and the experiments by P & L. In the next step, numerical simulations have been made of an axisymmetric turbulent jet diffusion hydrogen/air flame under the atmospheric pressure, by using a detailed chemistry model. We fulfill the numerical approach by using the thermodynamic and chemistry data from CHEMKIN-II. Detailed comparisons of temperature and major species have been conducted between the available experimental data [20] and the predicted results by the different combustion models coupled with the k–ε turbulence model and the ACC coupling model.

2. Turbulence model

In the present study, the motion of a Newtonian fluid is considered, governed by the Favre-averaged conservation equations for mass, momentum, enthalpy as follows [12]:

$$\frac{\partial \bar{\rho}}{\partial t} + \frac{\partial}{\partial x_j}(\bar{\rho}\tilde{u}_j) = 0 \tag{1}$$

$$\begin{aligned}\frac{\partial}{\partial t}(\bar{\rho}\tilde{u}_i) + \frac{\partial}{\partial x_j}(\bar{\rho}\tilde{u}_i\tilde{u}_j) &= -\frac{\partial}{\partial x_j}\left(\overline{\rho u_i'' u_j''}\right) \\ &+ \frac{\partial}{\partial x_j}\left(\mu\frac{\partial \tilde{u}_i}{\partial x_j}\right) - \frac{\partial \bar{\rho}}{\partial x_i} + (\bar{\rho}_0 - \bar{\rho})g\delta_{1i} \quad (i = 1, 2)\end{aligned} \tag{2}$$

where δ_{1i} is the Kronecker delta and g is the gravitation acceleration speed, $\overline{\rho u_i'' u_j''}$ is the Reynolds stress and modeled by the eddy viscosity assumption,

$$\overline{\rho u_i'' u_j''} = -\mu_t\left(\frac{\partial \tilde{u}_i}{\partial x_j} + \frac{\partial \tilde{u}_j}{\partial x_i} - \frac{2}{3}\delta_{ij}\frac{\partial \tilde{u}_k}{\partial x_k}\right) + \frac{2}{3}\bar{\rho}k\delta_{ij} \tag{3}$$

In addition, the conservation equations for the turbulent kinetic energy and its dissipation rate are modeled by the k–ε model as follows

$$\frac{\partial}{\partial t}(\bar{\rho}k) + \frac{\partial}{\partial x_j}(\bar{\rho}\tilde{u}_j k) = \frac{\partial}{\partial x_j}\left(\frac{\mu_{\text{eff}}}{\sigma_k}\frac{\partial k}{\partial x_j}\right) + G - \bar{\rho}\varepsilon \tag{4}$$

$$\begin{aligned}&\frac{\partial}{\partial t}(\bar{\rho}\varepsilon) + \frac{\partial}{\partial x_j}(\bar{\rho}\tilde{u}_j\varepsilon) \\ &= \frac{\partial}{\partial x_j}\left(\frac{\mu_{\text{eff}}}{\sigma_\varepsilon}\frac{\partial \varepsilon}{\partial x_j}\right) + C_1\frac{\varepsilon}{k}G - C_2\frac{\varepsilon^2}{k}\bar{\rho}\end{aligned} \tag{5}$$

where μ_t, μ, μ_{eff} are the turbulent viscosity, molecular viscosity and effective eddy viscosity, respectively; G is the production rate of the turbulent kinetic energy,

$$\mu_{\text{eff}} = \mu_t + \mu, \quad \mu_t = C_\mu\bar{\rho}\frac{k^2}{\varepsilon}$$

$$G = \mu_t\left(\frac{\partial \tilde{u}_j}{\partial x_i} + \frac{\partial \tilde{u}_i}{\partial x_j} - \frac{2}{3}\delta_{ij}\frac{\partial \tilde{u}_k}{\partial x_k}\right)\frac{\partial \tilde{u}_i}{\partial x_j}$$

In order to avoid overestimation of the jet spreading rate, the modified k–ε turbulence model employed in the present work involves the use of the Rodi correction [3] for the free jet modeling given by

$$C_\mu = 0.09 - 0.04c$$

$$C_2 = 1.92 - 0.0667c$$

where c is the mean flow retardation parameter defined as

$$c = \left(\frac{b}{U_s}\left|\frac{\partial U_s}{\partial x}\right|\right)^{0.2}$$

Here, U_s is the velocity at the jet centerline and b is the half-width of velocity for the jet.

3. Combustion model

The general set of N_r elementary reversible chemical reactions involving N_s chemical species A_i can be represented as follows:

$$\sum_{i=1}^{N_s} \nu'_{ij} A_i \rightleftharpoons \sum_{i=1}^{N_s} \nu''_{ij} A_i, \quad j = 1, 2, \ldots, N_r \tag{6}$$

where ν''_{ij} and ν'_{ij} is the ith species stoichiometric constants for the jth forward and backward reaction, respectively.

The conservation equation for the chemical species i is as follows

$$\frac{\partial}{\partial t}\left(\bar{\rho}\tilde{Y}_i\right) + \frac{\partial}{\partial x_j}\left(\bar{\rho}\tilde{u}_j\tilde{Y}_i\right) = \frac{\partial}{\partial x_j}\left[\left(\bar{\rho}D_{im} + \frac{\mu_t}{\sigma_{\tilde{Y}}}\right)\frac{\partial \tilde{Y}_i}{\partial x_j}\right] + \tilde{\dot{\omega}}_i \quad (i = 1, 2, \ldots, N_s) \tag{7}$$

where $\tilde{Y}_i$ is the mass fraction of the ith chemical species (here including nine species: H_2, O_2, H, O, OH, H_2O, HO_2, H_2O_2, N_2 for H_2/air flames); D_{im} is the mixture diffusion coefficient of species; $\sigma_{\tilde{Y}}$ is the turbulent Schmidt number; $\tilde{\dot{\omega}}_i$ is the net rate of creation of species i by chemical reaction and is given by,

$$\tilde{\dot{\omega}}_i = \tilde{\dot{\omega}}_i^+ - \tilde{\dot{\omega}}_i^- \tag{8}$$

where $\tilde{\dot{\omega}}_i^+$ and $\tilde{\dot{\omega}}_i^-$ are the production and destruction rates of species i as follows,

$$\tilde{\dot{\omega}}_i^+ = M_i \sum_{j=1}^{N_r}\left(\nu''_{ij}\tilde{R}_{f_j} + \nu'_{ij}\tilde{R}_{b_j}\right),$$
$$\tilde{\dot{\omega}}_i^- = M_i \sum_{j=1}^{N_r}\left(\nu'_{ij}\tilde{R}_{f_j} + \nu''_{ij}\tilde{R}_{b_j}\right) \tag{9}$$

where M_i is the molecular weight of the ith species; for the laminar flows, the forward and the backward reaction rates are determined as follows

$$R_{f_j} = \left(\sum_{i=1}^{N_s}\alpha_{ij}\tilde{C}_i\right)k_{f_j}\prod_{i=1}^{N_s}\tilde{C}_i^{\nu'_{ij}},$$
$$R_{b_j} = \left(\sum_{i=1}^{N_s}\alpha_{ij}\tilde{C}_i\right)k_{b_j}\prod_{i=1}^{N_s}\tilde{C}_i^{\nu''_{ij}} \tag{10}$$

where α_{ij} is the third body efficiency for the ith species in the jth reaction; $\tilde{C}_i = \bar{\rho}\tilde{Y}_i/M_i$ is the molar concentration of the ith species. The forward and backward reaction rate constants by the modified Arrhenius law are given by

$$k_{f_j} = A_{f_j}T^{B_{f_j}}e^{-E_{f_j}/R\tilde{T}}, \qquad k_{b_j} = \frac{k_{f_j}}{K_{C_j}} \tag{11}$$

where K_{C_j} is the equilibrium constant.

We choose an ACC model [13] for the coupling of turbulence and combustion. In this model, on the jth forward chemical reaction of a two species Y_1, Y_2, the turbulent reacting rate can be described as follows:

$$\widetilde{R_{f_j}} = B\bar{\rho}^2\widetilde{Y_1}\widetilde{Y_2}\exp\left(-\frac{E_{f_j}}{R\tilde{T}}\right)(1 + F_j)$$

$$F_j = \left[\frac{\widetilde{Y_1'Y_2'}}{\tilde{Y}_1\tilde{Y}_2} + \frac{E_{f_j}}{R\tilde{T}}\left(\frac{\widetilde{T''Y_1''}}{\tilde{T}\tilde{Y}_2} + \frac{\widetilde{T''Y_2''}}{\tilde{T}\tilde{Y}_2}\right) + \frac{1}{2}\frac{E_{f_j}}{R\tilde{T}}\frac{\tilde{T}'^2}{\tilde{T}^2}\right] + \alpha_{f_j}\left[\frac{\widetilde{T''Y_1'}}{\tilde{T}\tilde{Y}_1} + \frac{\widetilde{T''Y_2'}}{\tilde{T}\tilde{Y}_2} + \frac{E_{f_j}}{R\tilde{T}}\frac{\tilde{T}'^2}{\tilde{T}^2}\right]$$

where

$$\widetilde{Y_1''Y_2''} = C_y\frac{k^3}{\varepsilon^2}\frac{\partial\tilde{Y}_1}{\partial x_k}\frac{\partial\tilde{Y}_2}{\partial x_k},$$

$$\widetilde{T''Y_{1(2)}''} = C_{y1(2)}\frac{k^3}{\varepsilon^2}\frac{\partial\tilde{T}}{\partial x_k}\frac{\partial\tilde{Y}_{1(2)}}{\partial x_k},$$

$$\frac{\tilde{T}'^2}{\tilde{T}^2} = C_T\frac{k^3}{\varepsilon^2}\left(\frac{\partial\tilde{T}}{\partial x_k}\right)^2$$

The C_y, C_{y1}, C_{y2}, and C_T are the empirical constants and need to be optimized.

Detailed chemistry mechanism has been considered for the present turbulent hydrogen/air diffusion flame. The chemical reactions are described by nine chemical species and 16 pairs of reversible elementary steps. The chemical species considered are: H_2, O_2, H, O, OH, H_2O, HO_2, H_2O_2, (and N_2 as an inert substance). It is referred to as mechanism 1. The pre-exponential fraction A_{f_j}, the activation energy E_{f_j} and the temperature exponent of the pre-exponential factor

B_{f_j} are listed in Table 1 [21] for convenience. All species act equally as third bodies and the enhanced effective third body efficiency is equal to unity when a third body is required in the reaction. In addition to the above mechanism 1, another mechanism (referred as mechanism 2) including 17 reversible reactions is also used for the present simulation. Detailed data can be obtained from Ref. [6].

The density of species mixture can be calculated by the state equation of ideal gases. The enthalpy for chemically reacting flows is given as the weighted sum of each species mass fraction

$$\tilde{h} = \sum_{i=1}^{N_s} \tilde{Y}_i h_i = \sum_{i=1}^{N_s} \tilde{Y}_i \left(h_{f_i}^0 + \int_{T_{ref}}^{T} c_{pi}\, dT \right) \tag{13}$$

where $h_{f_i}^0$ is the heat formation of the ith species at the reference temperature of T_{ref} (=298.16 K); the last term of the integral part is the sensible heat.

The energy equation of enthalpy is written as

$$\frac{\partial}{\partial t}(\bar{\rho}\tilde{h}) + \frac{\partial}{\partial x_j}\left(\bar{\rho}\tilde{u}_j\tilde{h}\right) = \frac{\partial}{\partial x_j}\left[\left(\frac{\lambda}{c_p} + \frac{\mu_t}{\sigma_{\tilde{h}}}\right)\frac{\partial \tilde{h}}{\partial x_j}\right] + \frac{\partial}{\partial x_j}\left\{\sum_{i=1}^{N}\tilde{h}_i\left[\left(\bar{\rho}D_{im} + \frac{\mu_t}{\sigma_{\tilde{Y}}}\right) - \left(\frac{\lambda}{c_p} + \frac{\mu_t}{\sigma_{\tilde{h}}}\right)\right]\frac{\partial \tilde{Y}_i}{\partial x_j}\right\} \tag{14}$$

where $\sigma_{\tilde{h}}$ is the turbulent Prandtl number.

The temperature of the gas mixture must be implicitly calculated by solving Eq. (13) using the Newton–Raphson method because the specific heat c_{p_i} of the species is strongly dependent on temperature.

The general form of the transient transport equation for the 2D turbulent reactive flow under cylindrical coordinates can be written as

$$\frac{\partial}{\partial t}(\bar{\rho}\phi) + \frac{\partial}{\partial x}(\bar{\rho}\tilde{u}\phi) + \frac{1}{r}\frac{\partial}{\partial r}(r\bar{\rho}\tilde{v}\phi) = \frac{\partial}{\partial x}\left(\Gamma\frac{\partial \phi}{\partial x}\right) + \frac{1}{r}\frac{\partial}{\partial r}\left(r\Gamma\frac{\partial \phi}{\partial r}\right) + S_\phi \tag{15}$$

where ϕ denotes 1, $\tilde{u}$, $\tilde{v}$, k, ε, $\tilde{h}$, $\tilde{Y}_i$ and the general diffusion coefficient Γ is in turn 0, μ_t, μ_t, μ_{eff}/σ_k, $\mu_{eff}/\sigma_\varepsilon$, $\lambda/c_p + \mu_t/\sigma_{\tilde{h}}$ and $\bar{\rho}D_{im} + \mu_t/\sigma_{\tilde{Y}}$, respectively. Temperature- and species-dependence are imposed on the thermodynamic and transport property calculations. The thermochemical and transport properties are decoded from the CHEMKIN-II package. The constants entering into the turbulence and combustion models are listed as follows: $C_1 = 1.44\,(1.60)$, $C_2 = 1.92$, $C_\mu = 0.09$, $\sigma_{\tilde{h}} = \sigma_{\tilde{Y}} = 0.75$, $\sigma_k = 1.0$, $\sigma_\varepsilon = 1.3$, $C_y = C_{y1} = C_{y2} = C_T = 0.01$. It should be noted that for the calculation of turbulent diffusion flame, a higher value of $C_1 = 1.6$ is used for the case of turbulent diffusion flames.

4. Numerical schemes

Time-dependent Navier–Stokes equations are solved together with the species- and energy-conservation equations. The multi-grid method is used to accelerate converge [22]. The cylindrical velocity components are stored in a collocated grid system. The general form of

Table 1
Chemical kinetics for H_2/O_2 combustion[a]

j	Reactions considered	A_{f_j} (mol cm s)	B_{f_j}	E_{f_j} (cal/mol)
1	$H_2 + O_2 \rightleftarrows 2OH$	1.70E+13	0.0	47,780.0
2	$H_2 + OH \rightleftarrows H_2O + H$	1.17E+09	1.3	3626.0
3	$O_2 + H \rightleftarrows OH + O$	2.00E+14	0.0	16,800.0
4	$O + H_2 \rightleftarrows OH + H$	1.80E+10	1.0	8826.0
5	$H + O_2 + M \rightleftarrows HO_2 + M$	2.10E+18	−1.0	0.0
6	$OH + HO_2 \rightleftarrows H_2O + O_2$	5.00E+13	0.0	1000.0
7	$H + HO_2 \rightleftarrows 2OH$	2.50E+14	0.0	1900.0
8	$O + HO_2 \rightleftarrows O_2 + OH$	4.80E+13	0.0	1000.0
9	$OH + OH \rightleftarrows O + H_2O$	6.00E+08	1.3	0.0
10	$H_2 + M \rightleftarrows H + H + M$	2.23E+12	0.5	92,600.0
11	$O_2 + M \rightleftarrows O + O + M$	1.85E+11	0.5	95,560.0
12	$H + OH + M \rightleftarrows H_2O + M$	7.50E+23	−2.6	0.0
13	$H + HO_2 \rightleftarrows H_2 + O_2$	2.50E+13	0.0	700.0
14	$HO_2 + HO_2 \rightleftarrows H_2O_2 + O_2$	2.00E+12	0.0	0.0
15	$H_2O_2 + M \rightleftarrows OH + OH + M$	1.30E+17	0.0	45,500.0
16	$H_2O_2 + OH \rightleftarrows H_2O + HO_2$	1.00E+13	0.0	1800.0

[a] $k_{f_j} = A_{f_j} T^{B_{f_j}} \exp(-E_{f_j}/RT)$, $R = 1.987$ cal/(mol K).

Eq. (15) represents the conservation equations for the mass, axial and radial momentum, turbulent kinetic energy and its dissipation rate, enthalpy, and the mass fractions of species in cylindrical coordinates. The equations are solved sequentially with the SIMPLE method [23] to couple the pressure and velocity. At first, the axial and radial momentum equations are solved. After the pressure correction is calculated, the velocities and pressure are corrected in order to satisfy the continuity equation. The turbulent viscosity is calculated after the turbulent kinetic energy and its dissipation rate are solved. The enthalpy transport equation is subsequently solved and the temperature can be decoded from the enthalpy and the species by the Newton–Raphson method. Next, the chemical species equations are handled in an order of H_2, O_2, H, O, OH, H_2O, HO_2, H_2O_2, N_2 for the hydrogen/air flame. The N_2 mass fraction can be directly obtained by the global species conservation law. This process is repeated until the convergence criterion is achieved.

The finite volume integration of the transport equation of Eq. (15) is linearized and solved by the SIP (Strongly-Implicit-Procedure) method [24]. The relaxation technique is used to improve the convergence. The relaxation factor for the species equation must be selected much lower than that for other dependent-variable equations. The contribution of individual species via the reaction rate to the source term in a species equation is treated explicitly or implicitly according to the characteristic of the formation or destruction by each chemical reaction. This semi-implicit method is to preserve diagonal dominance and this is essential for a stable integration solution for multi-elementary reactions with multi-component species.

In the numerical investigations, four kinds of boundary conditions are selected. Fixed values are specified at the inlet of the fuel inject and the coflow air streams by the so-called Dirichlet boundary condition. At the outlet boundary far away from the nozzle exit, the Neumann boundary condition with the vanishing gradient is used for all variables such as the velocity components, pressure, enthalpy and species. At the unconfined air entrainment boundary, the pressure boundary condition is adopted, whereas the pressure is kept constant and the velocities are calculated from the continuity equation [25]. Symmetry boundary condition is imposed on the axis.

The numerical modeling procedure for the combusting flows with detailed chemistry is as follows: the combusting flow solutions with a global one-step chemical mechanism are first obtained and used as the initial conditions for the turbulent diffusion flame calculations with detailed chemistry. The time step is 10^{-4} s during the initial time steps of the calculation and is subsequently increased to 10 s after the flame achieves at a relatively steady state.

5. Results and discussion

5.1. Isothermal free jet flow

For validation, calculation is made of an air jet of 6.1 mm diameter at a Reynolds number of 1.1×10^4. The air fluid is issued with a uniform velocity profile into a quiescent air medium. The jet velocity is 27 m/s. The computational domain is 160 nozzle exit diameters in the axial direction and 30 diameters in the radial direction. Three-level of multi-grid with the finest grid of 81×81 is used. The calculations are compared with the experimental results by P & L [1].

Fig. 1 shows the predicted velocity profiles (U_{in}/U_s) using the standard and modified k–ε turbulence models compared with the experiments published by P & L [1], where U_{in} (being used as reference velocity) is the nozzle exit velocity and U_s is the centerline mean velocity. It can be seen that the Rodi correction compares much better to the experiments than the standard k–ε model. The predicted slope of the line is about 0.165 and compares well with the measured result. The velocity U_s decreases linearly with the axial distance from the nozzle exit. The half value radii b, i.e. the radius where the mean velocity is half the centerline value, is displayed in Fig. 2. The half-width b increases with the downstream location x and the centreline mean velocity is inversely proportional to x, which is caused by the jet spreading by entrainment of the surrounding air. The theoretical results [2] show a higher value of the centreline mean velocity and a lower value of the half-width.

The radial distribution of the axial velocity is found to be Gaussian, as shown in Fig. 3. The radial distribution of the turbulent kinetic energy at $x/d = 60$ is shown in Fig. 4. It can be found that Wygnanski and Fiedler presented much higher values near the centerline and lower values further away from the centerline. The agreements between the predicted results by the Rodi correction and the measurements by P & L are quite good. It is confirmed that the Rodi correction improves a lot of the mean velocity and the turbulent kinetic energy profiles across the jet. The turbulence intensity is about 25.5% at the centreline.

The distributions of the mean velocity, the Reynolds stress and the turbulence kinetic energy indicate that the radial profile becomes self-preserving within the range of $x/d = 60$–120 as shown in Fig. 5. It can be observed that the transverse velocity component is much smaller than the longitudinal velocity and the maximum shear stress

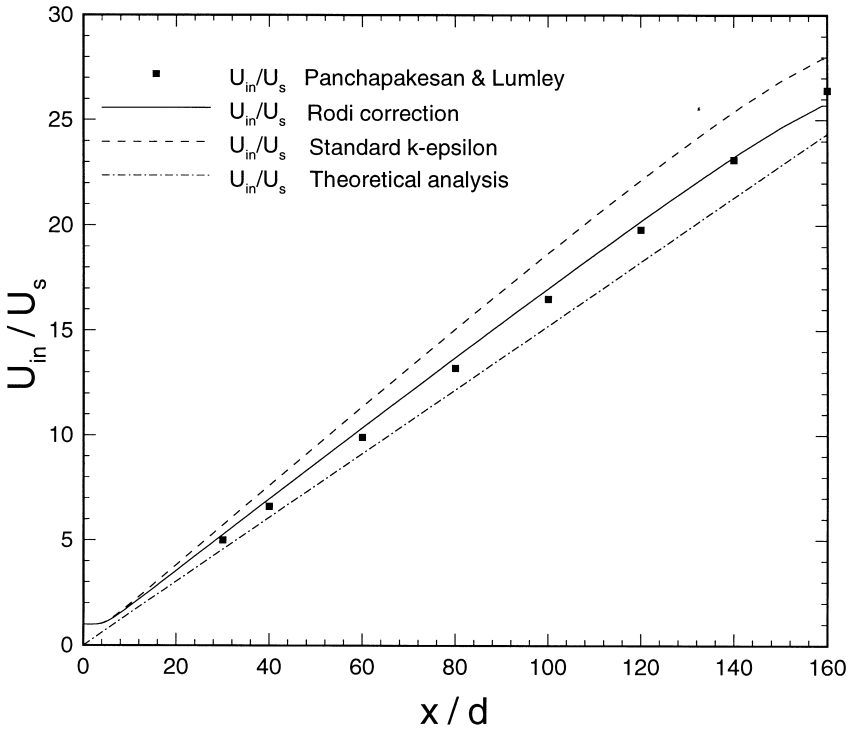

Fig. 1. Variation of centerline mean velocity for the isothermal free jet.

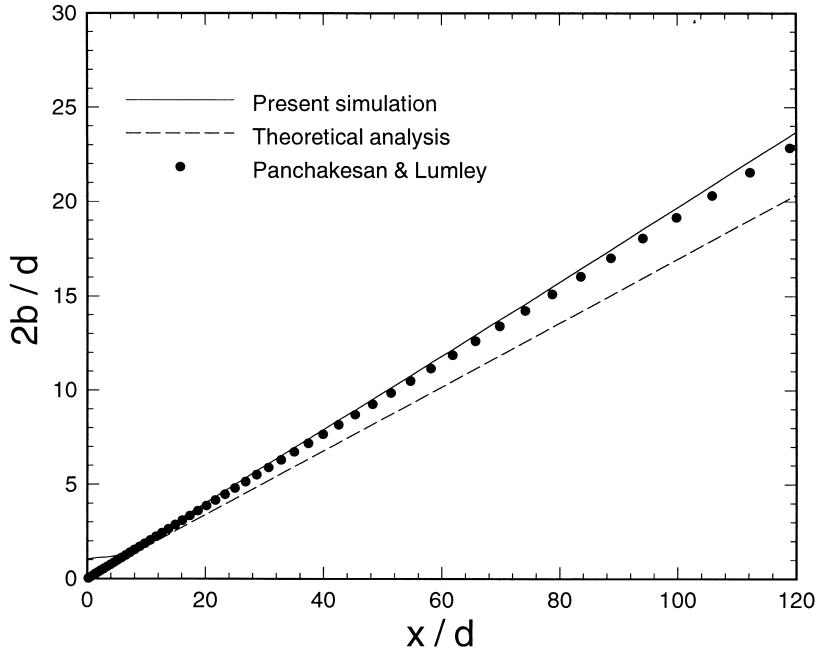

Fig. 2. Spreading of half value radii b for the isothermal free jet.

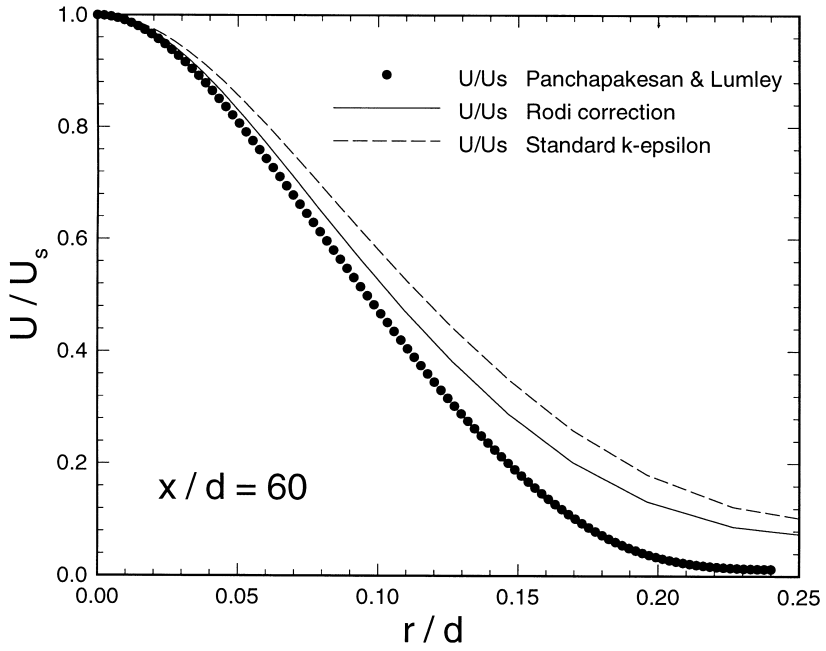

Fig. 3. Axial mean velocity profile across the jet at the axial location of $x/d = 60$.

$\langle uv \rangle / U_s^2$ and the maximum of the transverse velocity are located in the shear layer between the primary flow and the coflow. At $x/d = 120$ there are some deviations from self-similarity in the coflow region. This may be caused by the free-surface boundary condition near the outlet.

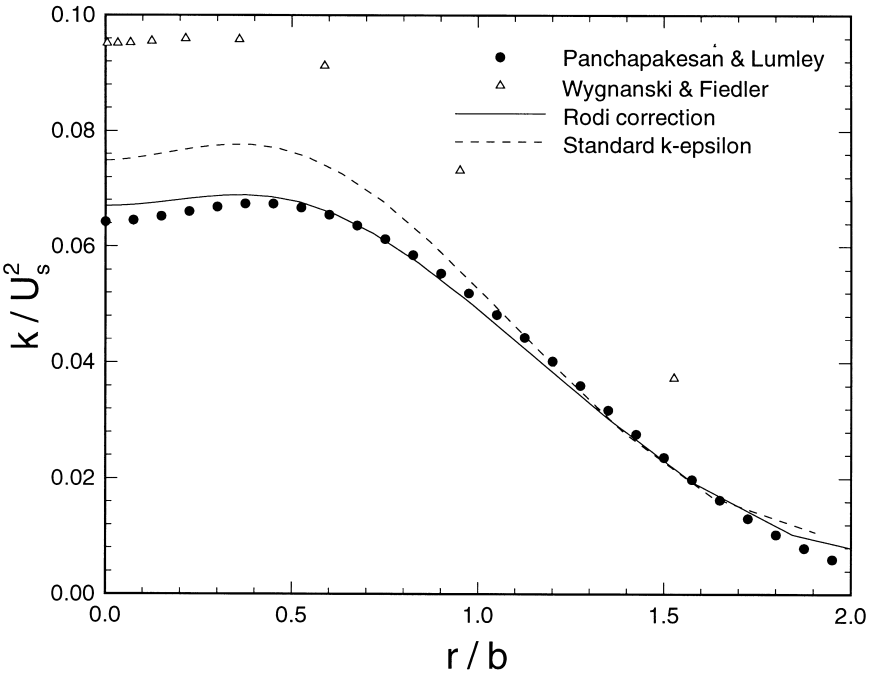

Fig. 4. Turbulence kinetic energy profile across the jet at the axial location in the fully developed region.

5.2. Turbulent diffusion flame

The experimental test case chosen to validate the present combustion model is the turbulent jet H_2/air diffusion flame which has been considered as a benchmark for validation in the proceedings of the International Workshop on Measurement and Computation of turbulent diffusion Flames held in Naples, Italy in 1996. A full data set is available in Ref. [20], which is comprised of the Favre-averaged temperature, mixture fraction, mass fractions of the major species (O_2, N_2, H_2, H_2O) and etc.

A mixture of 50% H_2 and 50% N_2 is discharged vertically upward from the round burner with a coflowing air stream. The burner is a tube with the inner diameter $D = 8$ mm and the outer diameter of 140 mm. The average velocity at the core tube exit is $U_{in} = 34.8$ m/s corresponding to a Reynolds number $Re = (\bar{\rho} U_{in} D)/\mu = 10{,}000$. The Froude number ($Fr = U_{in}^2/gD$) is 15,400. The surrounding coflow air velocity is 0.2 m/s. The turbulence intensity is 10% at the coflow inlet. The inlet temperature of the fuel (H_2/N_2) and air is 300 K. The turbulent kinetic energy and its dissipation rate at the tube exit are fitted to the LDA database provided by [20].

Calculations are made for the physical domain of 800 mm × 80 mm with a 241 × 61 non-uniform multi-grid system. Grid points are concentrated near the fuel tube. Fully developed velocity profiles are assumed at the primary exit of the central tube due to the fully developed turbulent pipe flow condition. A uniform velocity profile is set at the surrounding inlet stream. Grid independence is assessed by comparing different grids. The results of the computation are compared with the experiments published in [20].

Figs. 6–8 show the radial profiles of the Favre-averaged temperature and the species mass fractions at three axial locations ($x/D = 5, 20, 80$) with the mechanism 1. The influences of the general diffusion coefficients Γ of the energy and species equations can be shown. The solid lines represent the predicted results using $(\rho D + \mu_t/\sigma_{\tilde{Y}})$ for the species equation and $(\lambda/c_p + \mu_t/\sigma_{\tilde{h}})$ for the enthalpy equation as the diffusion coefficient. The dotted lines are the simulating results by using $\mu_t/\sigma_{\tilde{Y}}$ and $\mu_t/\sigma_{\tilde{h}}$ as the diffusion coefficients for the species and energy equations. The dots are the experimental results. The former method gives some improvements for the peak temperature location along the radial direction. The differences of these two methods become smaller further downstream of the flame (e.g. $x/D = 80$).

Figs. 6 and 7 show that temperature increases from the lower centerline value to a maximum and then decreases to the surrounding room temperature (300 K). The predicted position of the peak temperature in

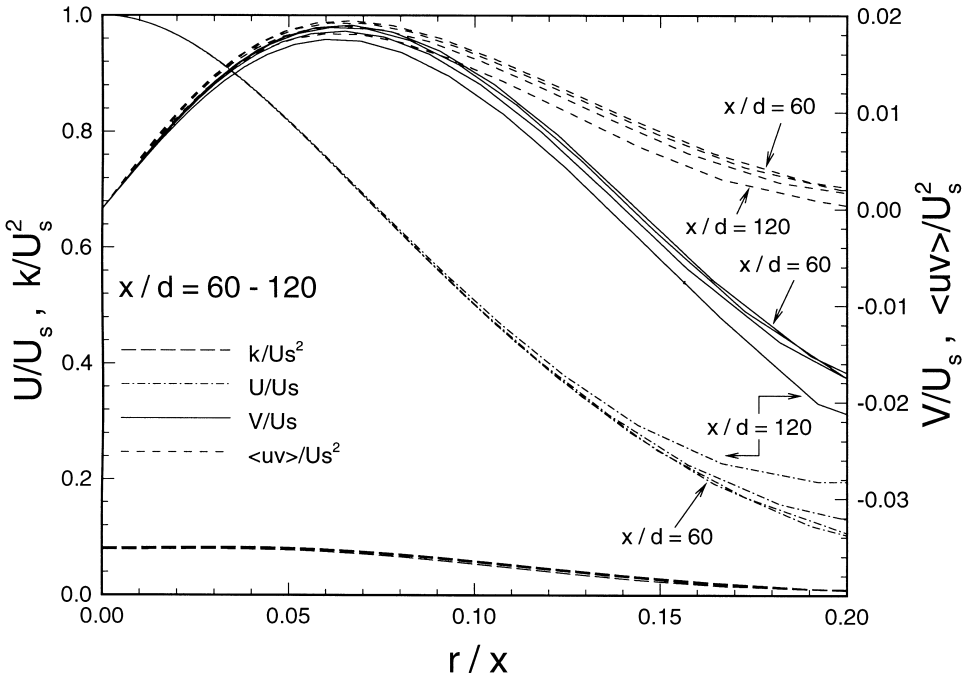

Fig. 5. Self-similar profiles of axial and radial mean velocity, turbulent kinetic energy and Reynolds stress across the jet at the axial locations of $x/d = 60$–120.

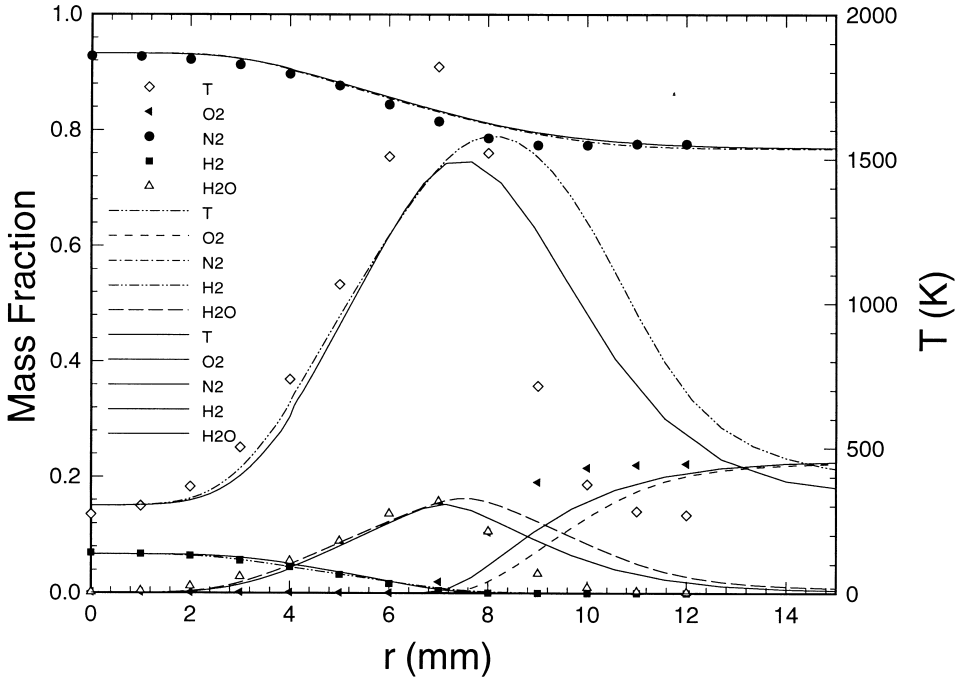

Fig. 6. Radial temperature and species profiles at the axial location of $x/D = 5$ by measurement and predictions with two kinds of diffusion coefficients.

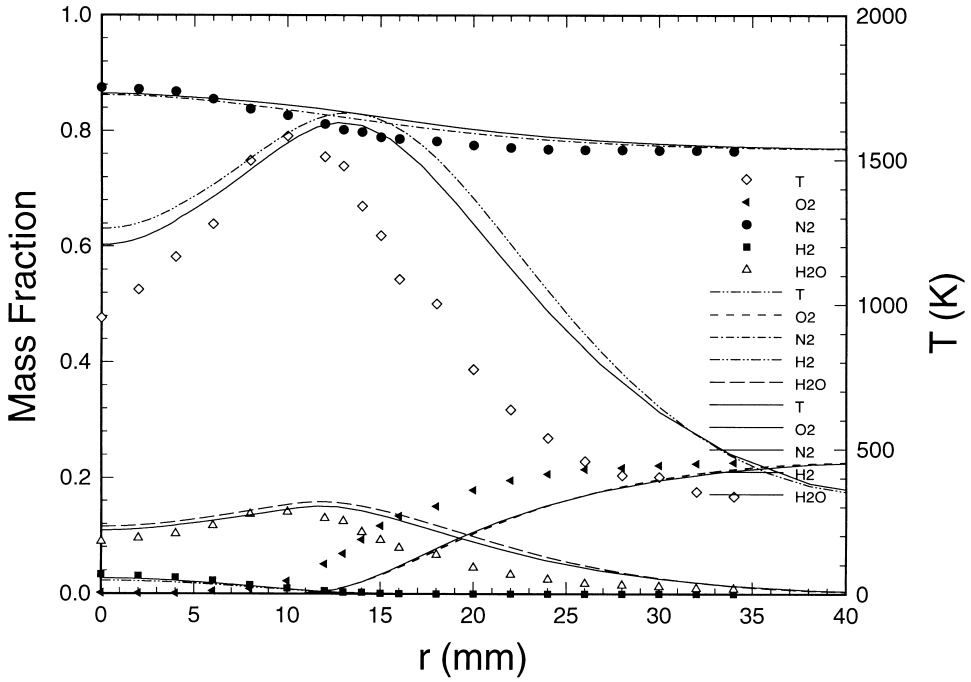

Fig. 7. Radial temperature and species profiles at the axial location of $x/D = 20$ by measurement and predictions with two kinds of diffusion coefficient.

the radial direction is further away from the centreline as compared to the experiment and this results in a delay of the decrease of the mass fraction of species H_2O and the increase of species O_2. The calculated H_2 concentration compares well with the experiment. The disagreement of the temperature and other species may be caused by an inaccurate diffusion or turbulent mixing with the co-flow O_2. The peak temperature is underpredicted at the axial position of $x/D = 5$ and is overpredicted at the axial position of $x/D = 20$. The maximum of H_2O is overpredicted and O_2 is underpredicted in the outer shear layer region due to the larger spreading. Fig. 7 shows that the predicted centreline temperature and the mass fraction of the species H_2O are higher and the mass fraction of the species H_2 is a little lower than the experiments. Fig. 8 shows that all of the H_2 has been consumed at this axial location above the tip of flame height (e.g. $x/D = 80$). The agreements between the experiments and computations are quite good for the major species. The temperature achieves its maximum value along with the maximum of H_2O and the minimum of O_2 located at the centerline. The predicted temperature is larger than the experiment, which may be caused by the radiation effect which has not been considered here.

The forms for the general diffusion coefficients for the species and energy equations suggested by Kim [12] are also utilized in the present simulation. But it is found that the forms, $\frac{\partial}{\partial x_j}\left[(D_{i\mathrm{m}} + \frac{\mu_t}{\sigma_{\tilde{Y}}})\frac{\partial(\bar{\rho}\tilde{Y}_i)}{\partial x_j}\right]$ used in the diffusion term of the species equation and $\rho(D_{i\mathrm{m}} + \mu_t/\sigma_{\tilde{Y}})$ used in the energy equation, lead to the false centerline distributions. From the dimensional unit analysis this method is also inaccurate because μ_t already involves the density $\bar{\rho}$.

Figs. 9 and 10 show the predicted radial profiles at $x/D = 40$ and the centreline distributions calculated by the two kinetic mechanisms (1 and 2) mentioned in the previous section. The dotted lines correspond to the simulation applying mechanism 1 and the solid lines by mechanism 2. Mechanism 1 gives a lower peak value of the temperature than mechanism 2, but the peak value location and the general trend of the flame are predicted without much differences. At $x/D = 40$ the radial profiles show the same trend as that at $x/D = 80$. The peak temperature is in good agreement with the experiment, but the prediction reveals a wider spreading. It can be seen from Fig. 10 that the predicted peak temperature location at the centerline is about $x/D = 32$ which is a slightly upstream from the experimental result. The agreements between the calculation and the experiment are quite good along the centreline.

It can be seen from the above figures that the predicted results compare much better along the radial direction at the downstream of the flame than

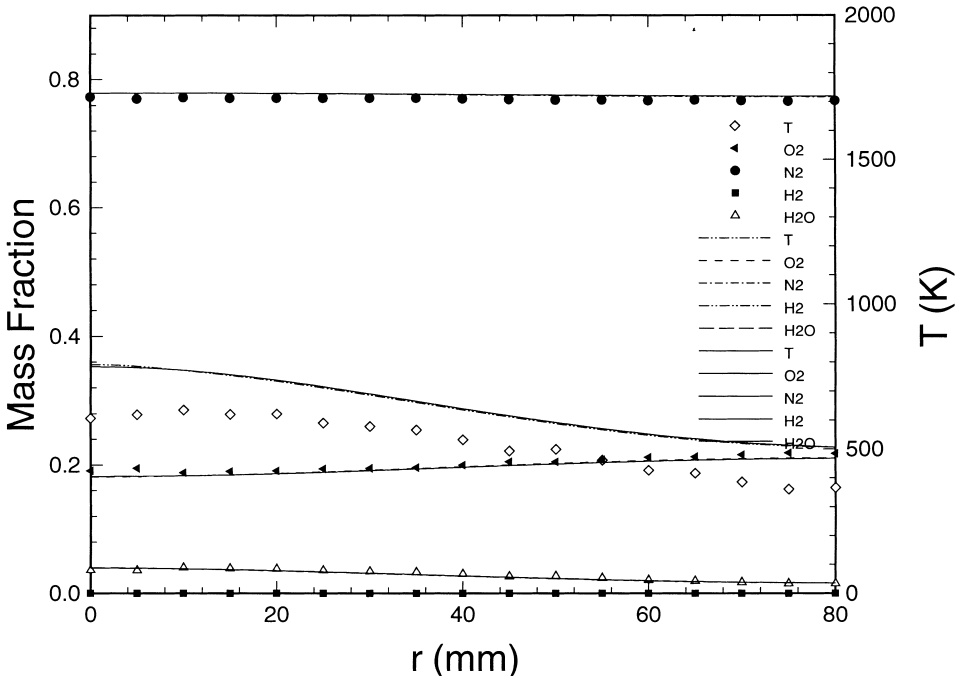

Fig. 8. Radial temperature and species profiles at the axial location of $x/D = 80$ by measurement and predictions with two kinds of diffusion coefficients.

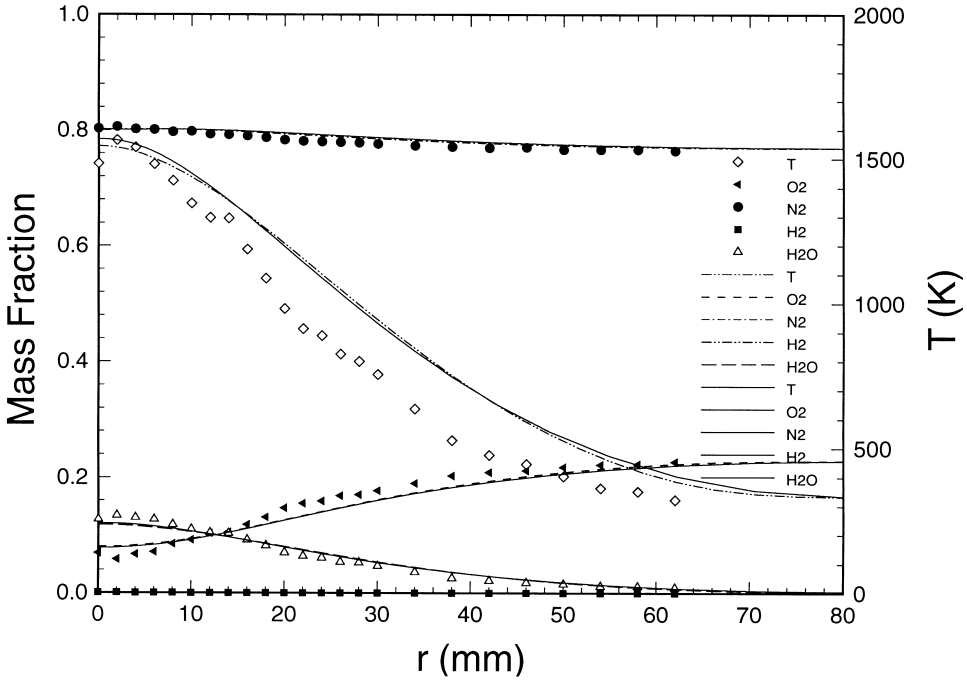

Fig. 9. Radial temperature and species profiles at the axial location of $x/D = 40$ by measurement and predictions with two kinds of chemical mechanism.

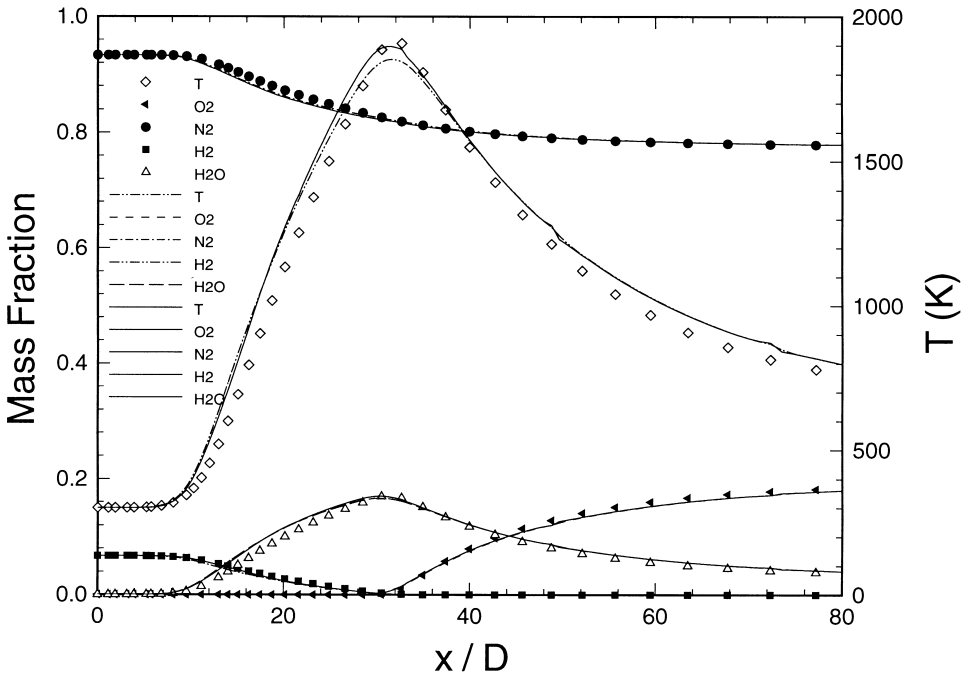

Fig. 10. Centerline temperature and species profiles by measurement and predictions with two kinds of chemical mechanism.

upstream near the fuel tube. The differences of the predictions using different kinds of the general diffusion coefficients become smaller further downstream of the flame. The radial temperature and species profiles become wider and flatter with increasing axial distance. In all cases, the peak mean temperature appears at the same position where the maximum mass fraction of H_2O occurs and the species O_2 and H_2 are almost consumed.

The selected approach delivers a good modeling quantity for the case investigated although a simple turbulence–combustion coupling model is used. It can be seen that the species H_2 and O_2 cannot coexist in most locations. The fast chemistry mechanism of 'mixed-and-burned' is expected to play an important role in the flame investigated. Chemistry takes place in thin layers where the chemical source term and the molecular transport are the leading terms, while outside the strongly-reactive zone the turbulent mixing dominates the flow field. A similar modeling quality can be expected for the hydrogen/air diffusion flames in which the fast chemistry dominates.

6. Conclusion

The first step of the present work is to model a free jet flow with the k–ε turbulent model to verify the numerical method. It shows that the Rodi correction improves the over-prediction of jet spreading by the standard k–ε model. The predicted results are compared well with the experiments by P & L. The basic characteristics of a round jet flow such as the self-similarity and jet spreading are well captured.

In addition, we report the application of multi-step elementary chemical reactions in modeling an axisymmetric turbulent hydrogen/air diffusion jet flame. The realistic physical property models and multi-component diffusion are included in the complex chemistry model. Distributions of the temperature and the major species (N_2, O_2, H_2, H_2O) along the radial and axial directions have been numerically investigated and compared with the experiments. The agreements of the temperature and major species are considered to be good between the predictions and the available measured data. The predicted results such as the peak temperature position depend on how the general diffusion coefficients for the energy and species equations are calculated. The peak temperature value along the radial direction is determined by the choice of the chemical mechanism. The present simulation gives wider radial profiles than the experiment at the upstream region, but it is compared well at further downstream location. Although the fluctuating quantities in the mean chemical reaction rates are modeled by a simple algebraic correlation closure (ACC) model, the selected approach still delivers an overall good modeling quantity for the case investigated.

The disagreements may be caused by the inaccurate turbulent mixing of chemical species which results in lower peak temperatures at the upstream and higher values downstream than the experiments. It is expected that some advanced turbulence–combustion model or non-constant turbulent Schmidt number for different species as well as the radiation model make some improvements.

Acknowledgements

This work is supported by the Alexander von Humboldt Foundation in Germany. The authors thank Dr. R.S. Barlow in Sandia National Laboratories for providing the Internet address for the experimental database. The reviewer's recommendations and hints are also appreciated.

References

[1] N.R. Panchapakesan, J.L. Lumley, Turbulence measurements in axisymmetric jets of air and helium. Part 1: air jet, J. Fluid Mech. (246) (1993) 197–223.
[2] H. Schlichting, Boundary-Layer Theory, McGraw-Hill, New York, 1987.
[3] W. Rodi, Turbulence Models and Their Application in Hydraulics — A State of the Art Review, IAHR, Delft, 1980.
[4] I. Wygnanski, H. Fiedler, Some measurements in the self-preserving jet, J. Fluid Mech. (38) (1969) 577–612.
[5] A. Neuber, G. Krieger, M. Tacke, E. Hassel, J. Janicka, Finite rate chemistry and NO molefraction in non-premixed turbulent flames, Combustion and Flame 113 (1998) 198–211.
[6] V.R. Katta, L.P. Goss, W.M. Roquemore, Effect of nonunity Lewis number and finite-rate chemistry on the dynamics of a hydrogen–air jet diffusion flame, Combustion and Flame (96) (1994) 60–74.
[7] V.R. Katta, W.M. Roquemore, Numerical investigations of transitional H_2/N_2 jet diffusion flames, AIAA J 32 (1) (1994) 84–94.
[8] T. Takagi, Z. Xu, M. Komiyama, Preferential diffusion effects on the temperature in usual and inverse diffusion flames, Combustion and Flame 106 (1996) 252–260.
[9] J. Janicka, N. Peters, Prediction of turbulent jet diffusion flame lift-off using a PDF transport equation, in: Nineteenth Symposium (Int.) on Combustion, 1982, pp. 367–374.
[10] S.B. Pope, PDF methods for turbulent reactive flows, Progress in Energy and Combustion Science 11 (2) (1985) 119–192.
[11] N. Peters, Laminar flamelet concepts in turbulent combustion, in: Twenty First-Symposium (Int.) on Combustion, 1986, pp. 1231–1250.

[12] S.W. Kim, Numerical investigation of chemical reaction-turbulence interaction in compressible shear layers, Combustion and Flame 101 (1995) 197–208.
[13] L.X. Zhou, Theory and Numerical Modeling of Turbulent Gas-particle Flows and Combustion, Science/CRC press, Beijing, 1993.
[14] N. Branley, W.P. Jones, Large eddy simulation of a turbulent non-premixed flame, in: Proceedings of the Eleventh Symposium on Turbulent Shear Flows, Grenoble, France, 1997, pp. 21.1–21.6.
[15] S.H. Frankel, V. Adumitroaie, C.K. Madnia, P. Givi, Large-eddy simulation of turbulent reacting flows by assumed PDF methods, in: Engineering Application of Large Eddy Simulations, ASME, New York, 1993, pp. 81–101.
[16] U. Schumann, Large eddy simulation of turbulent diffusion with chemical reactions in the convective boundary layer, Atoms. Environ 23 (1989) 1–15.
[17] C.J. Montgomery, G. Kosaly, J.J. Riley, Direct numerical solution of turbulent nonpremixed combustion with multistep hydrogen–oxygen kinetics, Combustion and Flame 109 (1997) 113–144.
[18] R.S. Barlow, C.D. Carter, Relationship among nitric oxide, temperature, and mixture fraction in hydrogen jet flames, Combustion and Flame 104 (1996) 288–299.
[19] W. Meier, A.O. Vyrodov, V. Bergmann, W. Stricker, Simultaneous Raman/LIF measurements of major species and NO in turbulent H_2/air diffusion flames, Appl. Phys. B (63) (1996) 79–90.
[20] (http://www.th-darmstadt.de/fb/mb/ekt/flamebase/H3flame).
[21] A. Ern, V. Giovangigli, in: Multicomponent Transport Algorithms, Springer-Verlag, Berlin, 1984, p. 408.
[22] F. Durst, M. Schaefer, Parallel block-structured multigrid method for the prediction of incompressible flows, Int. J. Num. Methods Fluids (22) (1996) 549–565.
[23] S.V. Patankar, Numerical Heat Transfer and Fluid Flow, Hemisphere/McGraw-Hill, Washington/New York, 1980.
[24] H.L. Stone, Iterative solution of implicit approximations of multidimensional partial differential equations, SIAM J. Numer. Anal 5 (1968) 530–558.
[25] J.H. Ferziger, M. Peric, Computational Methods for Fluid Dynamics, Springer-Verlag, Berlin, Heidelberg, 1996.